
FAST FLUID SIMULATIONS IN 3D WITH PHYSICS-INFORMED DEEP LEARNING

PREPRINT

Nils Wandel

Department of Computer Science
University of Bonn
wandel@cs.uni-bonn.de

Michael Weinmann

Department of Computer Science
University of Bonn
mw@cs.uni-bonn.de

Reinhard Klein

Department of Computer Science
University of Bonn
rk@cs.uni-bonn.de

December 23, 2020

ABSTRACT

Physically plausible fluid simulations play an important role in modern computer graphics. However, in order to achieve real-time performance, computational speed needs to be traded-off with physical accuracy. Surrogate fluid models based on neural networks are a promising candidate to achieve both: fast fluid simulations and high physical accuracy. However, these approaches do not generalize to new fluid domains, rely on massive amounts of training data or require complex pipelines for training and inference.

In this work, we present a 3D extension to our recently proposed fluid training framework, which addresses the aforementioned issues in 2D. Our method allows to train fluid models that generalize to new fluid domains without requiring fluid simulation data and simplifies the training and inference pipeline as the fluid models directly map a fluid state and boundary conditions at a moment t to a subsequent state at $t+dt$. To this end, we introduce a physics-informed loss function based on the residuals of the Navier-Stokes equations on a 3D staggered Marker-and-Cell grid. Furthermore, we propose an efficient 3D U-Net based architecture in order to cope with the high demands of 3D grids in terms of memory and computational complexity. Our method allows for real-time fluid simulations on a $128 \times 64 \times 64$ grid that include various fluid phenomena such as the Magnus effect or Kármán vortex streets, and generalize to domain geometries not considered during training. Our method indicates strong improvements in terms of accuracy, speed and generalization capabilities over current 3D NN-based fluid models.

1 Introduction

Numerous applications in graphics and engineering rely on fast and stable fluid simulations. While physical correctness is of utmost importance for engineering applications like aerodynamic design, applications in computer graphics such as simulations for games or movies particularly focus on computational efficiency under the constraint of producing visually plausible results, thereby sacrificing physical accuracy by means of introducing pseudo-forces in order to get more appealing curls or using a physically-inaccurate notion of viscosity as well as due to numerical dissipation.

As solving the equations of fluid dynamics based on numerical approximation schemes comes at high computational costs that cannot be handled in real time, recent developments particularly focused on exploiting the potential of deep learning in the context of surrogate fluid solvers to significantly reduce the computational burden while maintaining a high physical accuracy [1, 2, 3, 4, 5]. Grid-based, physics-informed learning strategies even have been shown to allow CNNs to advance a fluid state in time efficiently and to generalize well to new domain geometries that are not contained in the training set [1, 2]. On top of that, the approach by Wandel et al. [2] can handle viscous fluids and dynamic boundary conditions while not relying on the availability of training data from fluid simulations in contrast to the approach by Tompson et al. [1]. Nevertheless, this method is limited to simulations in 2D domains and, hence, not suitable for the description of general 3D fluid behavior since symmetry along the third dimension cannot be expected in general. Using 3D grids, in turn, comes at the cost of significantly increasing computational complexity and memory

requirements. Additional challenges are given by the increasing number of degrees of freedom for 3D fluid motion as well as the more complex boundary conditions in 3D domains.

In this paper, we address these challenges by a novel unsupervised approach of learning incompressible fluid dynamics, i.e. how a fluid state at timestep t changes to a subsequent state at timestep $t+dt$, in 3D. For this purpose, we represent the fluid on a 3D staggered marker-and-cell grid and formulate a physics-informed loss function by penalizing residuals of the Navier-Stokes equations on this representation. We test our method on a 3D U-Net architecture and, to meet the demands for real-time performance, we also propose an efficient 3D-CNN-based architecture. This allows for fluid simulations on a $128 \times 64 \times 64$ grid at 37 timesteps per second while taking into account various fluid phenomena such as the Magnus effect and Kármán vortex streets. Furthermore, our framework allows to generalize to 3D domain geometries not considered during training and does not rely on previously generated fluid data, hence, significantly increasing its practical relevance as there is no need to consider large amounts of data from fluid solvers such as FEniCS, OpenFOAM or Mantaflow for the training of the fluid model. As demonstrated by our experiments, our method indicates strong improvements in terms of accuracy, speed and generalization capabilities compared to existing deep learning based approaches. Furthermore, we provide code and data for reproducing our method on `code_released_upon_acceptance`.

2 Related Work

In recent years, the rapid progress in deep learning inspired several approaches to approximate the dynamics of partial differential equations (PDEs) with efficient, learning-based surrogate models.

Lagrangian methods such as smoothed particle hydrodynamics (SPH) [6] model fluids based on a large number of individual particles that move with the fluid’s velocity field, i.e. each particle has different properties like mass or velocity. As a result, the conservation of mass can be easily preserved. Respective Lagrangian learning-based approaches for fluid simulation have been proposed based on regression forests [7], graph neural networks [8, 9] and continuous convolutions [10]. Furthermore, differentiable fluid simulations have been achieved based on Smooth Particle Networks (SP-Nets) [11]. Whereas Lagrangian methods are particularly suitable for fluid domains with large, dynamic surfaces such as waves or droplets, the accurate simulation of fluid dynamics within a fluid domain usually can be better achieved with *Eulerian methods*.

Eulerian methods model fluid properties such as the fluid’s velocity or pressure field on a fixed frame of reference. This includes methods that describe the fluid state using implicit neural representations, finite elements or grid-structures.

Continuous Eulerian methods map domain coordinates (e.g. x,y,t) directly onto field values (e.g. velocity \vec{v} / pressure p) using e.g. implicit neural representations, thereby allowing for mesh-free solutions ([12, 13, 14]). Respective applications include the modeling of flow through porous media ([15, 16, 17]), fluid modeling ([18, 19]), turbulence modeling ([20, 21]) and modeling of molecular dynamics ([22]). Such learning-based approaches typically involve a training process that includes a physics-informed loss function to penalize residuals of the underlying PDEs.

Furthermore, similar to our approach, Raissi et al. [23] focused on the approximation of the incompressible Navier-Stokes equations based on leveraging vector potentials to obtain continuous divergence-free velocity fields. While such continuous methods allow smooth and accurate simulations as well as overcoming the curse of dimensionality of discrete techniques in high-dimensional PDEs ([13]), the training of the respective networks relies on a specific domain. Hence, these networks are not capable of generalizing to new domains or being used in interactive scenarios.

In contrast, *discrete Eulerian methods* solve the underlying PDEs on a grid. While seminal work has been published decades ago [24, 25], recent techniques particularly focus on leveraging the potential of deep learning techniques to achieve speed ups while maintaining accuracy. Frameworks to learn parameterized fluid simulations [4] allow an efficient interpolation between such simulations. Furthermore, a RNN-GAN has been used to produce turbulent flow fields within a pipe domain [26]. However, in both cases, a generalization to new domain geometries not considered during training has not been achieved. The tempoGAN introduced by Xi et al. [27] allows temporally consistent super-resolution in the context of smoke simulations, producing plausible high-resolution smoke-density fields for low-resolution inputs. This, however, is not in accordance with our goal to obtain a fluid model that provides complete fluid state representations including velocity and pressure fields. With a focus on accelerating the simulation of Eulerian fluids, Tompson et al. [1] have shown how a Helmholtz projection step can be learned. While this method is capable to generalize to domain geometries not considered during training, the technique relies on a particle tracer to deal with the advection term of the Navier-Stokes equations. In addition, characteristic effects such as the Magnus effect or Kármán vortex streets cannot be simulated since Eulerian fluids do not model viscosity and dynamics boundary conditions were not considered. Discarding the pressure term in the Navier-Stokes equation, Geneva et al. [5] introduced

a physics-informed framework to learn the update step for the Burgers equations. Thuerey et al. [28] proposed to learn solutions of the Reynolds-averaged Navier-Stokes equations for airfoil flows. However, their approach does not generalize beyond airfoil flows and Reynolds-averaged Navier-Stokes equations do not model the temporal evolution of a fluid state. Furthermore, Um et al. [3] focused on learning a correction step so that solutions of a high-resolution fluid simulation can be approximated by a low-resolution differentiable fluid solver. However, generalization to new domain geometries has not been demonstrated.

Our approach also falls into this category of discrete Eulerian approaches. However, unlike the aforementioned approaches, our approach does not rely on the availability of vast amounts of data from fluid-solvers such as FEniCS, OpenFOAM or Mantaflow and handles dynamic boundary conditions allowing for interactions with the fluid in 3D.

3 Method

In this section, we first provide details regarding the underlying physical relationship described in terms of the incompressible Navier-Stokes equations. This is followed by a review of the Helmholtz decomposition that can be used to ensure the incompressibility within the fluid domain. After the discussion of these basic principles, we provide the details of our discrete model for fluid dynamics and show how a physics-informed loss function in terms of the residuals of the Navier-Stokes equations can be used to learn fluid dynamics.

3.1 Incompressible Navier-Stokes Equations

The Navier-Stokes equations have been shown to be a very good model for the dynamics of most incompressible fluids. If we consider the state of an incompressible fluid consisting of a velocity field \vec{v} and a pressure field p on a fluid domain Ω , then, the incompressible Navier-Stokes equations describe its evolution over time by a set of two partial differential equations, which are often referred to as incompressibility equation and momentum equation. The *incompressibility equation* ensures incompressibility of the fluid by enforcing that \vec{v} is divergence-free:

$$\nabla \cdot \vec{v} = 0 \text{ in } \Omega \quad (1)$$

The *momentum equation* ensures conservation of momentum within the fluid:

$$\rho \dot{\vec{v}} = \rho \left(\frac{\partial \vec{v}}{\partial t} + (\vec{v} \cdot \nabla) \vec{v} \right) = -\nabla p + \mu \Delta \vec{v} + \vec{f} \text{ in } \Omega \quad (2)$$

Here, ρ denotes the fluid density and μ the viscosity. The left-hand side of this equation can be interpreted as the change in momentum of fluid particles and the right-hand side represents the sum of the forces acting on them. These forces include the pressure gradient ∇p , viscous friction $\mu \Delta \vec{v}$ and external forces \vec{f} . In this work, we set $\vec{f} = 0$ since external forces such as e.g. gravity can be neglected.

On top of ensuring incompressibility and conservation of momentum within Ω , we also have to match initial conditions \vec{v}^0 and p^0 at the beginning of the simulation and fulfill Dirichlet boundary (no-slip) conditions at the boundary of the domain $\partial\Omega$. The Dirichlet boundary conditions state that the velocity field \vec{v} has to match the velocity \vec{v}_d at the domain boundaries, i.e.:

$$\vec{v} = \vec{v}_d \quad \text{on } \partial\Omega \quad (3)$$

3.2 Ensuring Incompressibility using a Vector Potential

The Helmholtz theorem states that every vector field \vec{v} can be decomposed into a curl-free and a divergence-free part, i.e.:

$$\vec{v} = \nabla q + \nabla \times \vec{a} \quad (4)$$

Note that ∇q is curl-free ($\nabla \times (\nabla q) = \vec{0}$) and $\nabla \times \vec{a}$ is divergence-free ($\nabla \cdot (\nabla \times \vec{a}) = 0$).

A common method to ensure incompressibility is to project \vec{v} onto its divergence free part by solving the Poisson problem $\nabla \cdot \vec{v} = \Delta q$ followed by subtracting ∇q from \vec{v} [25, 1]. Solving the Poisson problem, however, comes at high computational costs. Approximate, learned solutions [1] cannot guarantee proper projections onto the divergence-free part and thus might not fulfill incompressibility within the domain exactly.

For this reason, we follow the approaches of [23, 4, 2] and aim to directly predict a vector potential \vec{a} and set $\vec{v} = \nabla \times \vec{a}$. This guarantees incompressibility within the domain and automatically solves Equation 1.

3.3 Discrete Spatio-temporal 3D Fluid Representation

In order to process the fluid state with a 3D convolutional neural network, we consider the following spatial and temporal discretizations:

$$\vec{a} = \begin{pmatrix} (a_x)_{i,j,k}^t \\ (a_y)_{i,j,k}^t \\ (a_z)_{i,j,k}^t \end{pmatrix}; \vec{v} = \begin{pmatrix} (v_x)_{i,j,k}^t \\ (v_y)_{i,j,k}^t \\ (v_z)_{i,j,k}^t \end{pmatrix}; p = p_{i,j,k}^t \quad (5)$$

The relationship between \vec{a} , \vec{v} and p can be efficiently represented by arranging the discretized quantities on a Marker-And-Cell (MAC) grid as depicted in Figure 1a. This grid representation allows us to compute gradients, divergence, curl and Laplace operations for the Navier-Stokes equations in a straight forward manner.

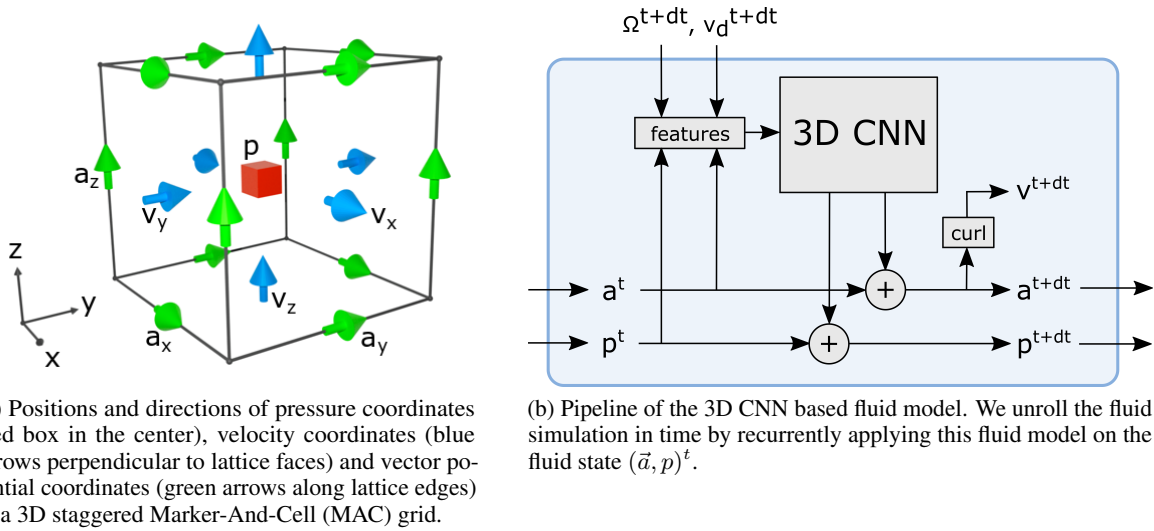


Figure 1: 3D MAC grid and diagram of the fluid model.

To calculate the velocity field $\vec{v} = \nabla \times \vec{a}$ of a vector potential \vec{a} on a MAC grid in 3D, we have to compute the curl as follows:

$$\begin{pmatrix} (v_x)_{i,j,k} \\ (v_y)_{i,j,k} \\ (v_z)_{i,j,k} \end{pmatrix} = \begin{pmatrix} (a_z)_{i,j+1,k} - (a_z)_{i,j,k} - (a_y)_{i,j,k+1} + (a_y)_{i,j,k} \\ (a_x)_{i,j,k+1} - (a_x)_{i,j,k} - (a_z)_{i+1,j,k} + (a_z)_{i,j,k} \\ (a_y)_{i+1,j,k} - (a_y)_{i,j,k} - (a_x)_{i,j+1,k} + (a_x)_{i,j,k} \end{pmatrix} \quad (6)$$

The divergence of the velocity field \vec{v} can be computed as follows:

$$\nabla \cdot \vec{v}_{i,j,k} = (v_x)_{i+1,j,k} - (v_x)_{i,j,k} + (v_y)_{i,j+1,k} - (v_y)_{i,j,k} + (v_z)_{i,j,k+1} - (v_z)_{i,j,k} \quad (7)$$

$$= 0 \quad (8)$$

By plugging the results from Equation 6 into Equation 7, you immediately arrive at Equation 8 (\vec{v} is divergence-free and the fluid thus incompressible).

For the Laplace operation, we use a convolution with the 27-point stencil by [29].

The temporal derivative in Equation 2 is handled as follows:

$$\rho \left(\frac{\vec{v}^{t+dt} - \vec{v}^t}{dt} + (\vec{v}^{t'} \cdot \nabla) \vec{v}^{t'} \right) = -\nabla p^{t+dt} + \mu \Delta \vec{v}^{t'} + \vec{f} \quad (9)$$

In literature, there are several different methods to assign $\vec{v}^{t'}$. The explicit method sets $\vec{v}^{t'} = \vec{v}^t$ whereas the implicit method sets $\vec{v}^{t'} = \vec{v}^{t+dt}$. Here, we focus on an implicit-explicit (IMEX) scheme that sets $\vec{v}^{t'} = \frac{\vec{v}^t + \vec{v}^{t+dt}}{2}$.

3.4 Fluid Model

Building upon this discrete representation, we now introduce a recurrent model for fluid dynamics, F , that maps the fluid state specified by the vector potential \vec{a}^t and the pressure field p^t at time point t to its subsequent state \vec{a}^{t+dt} and p^{t+dt} at time-point $t + dt$, given the domain Ω^{t+dt} with boundary conditions $\vec{v}^{t+dt} = \vec{v}_d^{t+dt}$:

$$(\vec{a}, p)^{t+dt} = F((\vec{a}, p)^t, \Omega^{t+dt}, \vec{v}_d^{t+dt}) \quad (10)$$

By recurrently applying F on the initial fluid state (\vec{a}^0, p^0) , the fluid simulation can be unrolled in time for given boundary conditions (Ω^t, \vec{v}_d^t) :

$$(\vec{a}, p)^{n \cdot dt} = F(\dots F((\vec{a}, p)^0, \Omega^{dt}, \vec{v}_d^{dt}) \dots, \Omega^{n \cdot dt}, \vec{v}_d^{n \cdot dt}) \quad (11)$$

Figure 1b gives an overview over the fluid model F . First, a feature representation is build based on the inputs that contains $(p^t, a^t, \nabla \times a^t, \Omega^{t+dt}, \partial\Omega^{t+dt}, \Omega^{t+dt} \cdot \nabla \times a^t, \Omega^{t+dt} \cdot p^t, \partial\Omega^{t+dt} \cdot \vec{v}_d^{t+dt})$ and can be efficiently computed with convolutions. Here, the boundary $(\partial\Omega)$ is simply set to $1 - \Omega$. These features are then fed into a 3D CNN. We can make arbitrary choices for the 3D CNN and tested 2 different variants: a 3D U-Net [30] version for accurate simulations and a pruned 3D U-Net version that is less accurate but considerably faster. For this smaller model we replaced concatenations with sums and removed 2 pooling stages as well as hidden layers at every stage. The output of the 3D CNN is then mean-normalized to prevent drifting offsets of \vec{a} and p and then added to the previous state of \vec{a}^t and p^t to obtain the fluid state of the next timestep \vec{a}^{t+dt} and p^{t+dt} .

3.5 Physics-informed Loss Function

In the following, we introduce a loss function based on the residulas of the Navier-Stokes equations (Equations 1 and 2) as well as the boundary conditions (see Equation 3). As incompressibility is already fulfilled by the vector potential, we do not have to introduce a loss term for Equation 1. For the momentum equation (Equation 9), we formulate the following momentum loss term:

$$L_p = \left\| \rho \left(\frac{\vec{v}^{t+dt} - \vec{v}^t}{dt} + (\vec{v}^{t'} \cdot \nabla) \vec{v}^{t'} \right) + \nabla p^{t+dt} - \mu \Delta \vec{v}^{t'} - \vec{f} \right\|^2 \text{ in } \Omega \quad (12)$$

Furthermore, the compliance of the Dirichlet boundary conditions (Equation 3) is enforced by a boundary loss term:

$$L_b = \left\| \vec{v}^{t+dt} - \vec{v}_d^{t+dt} \right\|^2 \text{ on } \partial\Omega \quad (13)$$

Combining the described loss terms, we obtain the following loss function:

$$L = \alpha L_p + \beta L_b \quad (14)$$

α and β are hyperparameters to weight the different loss terms. We chose $\alpha = 1$ and $\beta = 20$, because errors in L_b lead to very unrealistic fluxes penetrating the boundaries. Note that in contrast to solving the Navier-Stokes equations explicitly, computing these loss terms can be done very efficiently by convolutions in $O(N)$ where N corresponds to the number of grid cells.

3.6 Training Strategy

To start training, we initialize a pool $\{\Omega_k^0, (\vec{v}_d)_k^0, (a_z)_k^0, p_k^0\}$ of randomized domains Ω_k^0 , boundary conditions $(\vec{v}_d)_k^0$ and initial states for the vector potential and pressure field $(a_z)_k^0$ and p_k^0 . The randomized domains contain primitive shapes such as boxes, square rods or spinning cylinders and balls and the resolution of these domains is 128x64x64 voxels. For simplicity, all initial states are set to 0 ($(a_z)_k^0 = 0$ and $p_k^0 = 0$). Note that in contrast to all other 3D grid based training methods (including [1, 5]) we do not need any simulated fluid-data.

For every training step, we draw a random mini-batch $\{\Omega_k^t, (v_d)_k^t, (a_z)_k^t, p_k^t\}_{\{k \in \text{minibatch}\}}$ (batch size = 14) from the pool and feed it into the neural network. Then, the neural network is asked to predict the velocity ($\vec{v}_k^{t+dt} = \nabla \times \vec{a}_k^{t+dt}$) and pressure (p_k^{t+dt}) fields of the next time step. Based on a physics-informed loss-function (Equation 14), we update the weights of the network using the Adam optimizer ([31]) (learning rate=0.0005). At the end of each training step, the pool is updated by replacing the old vector potential and pressure fields $(a_z)_k^t, p_k^t$ by the newly predicted ones $(a_z)_k^{t+dt}, p_k^{t+dt}$. This recycling strategy fills the training pool with more and more realistic fluid states as the model becomes better at simulating fluid dynamics.

From time to time, old environments of the training pool are replaced by new randomized environments and the vector potential as well as the pressure fields are reset to 0. This increases the variance of the training pool and helps the neural network to learn "cold starts" from $\vec{0}$ -velocity and 0-pressure fields.

For the implementation of both models, we used the popular machine learning framework Pytorch and trained the models on a NVidia GeForce RTX 2080 Ti. Training converged after about 3 days.

4 Results

In the following, we present qualitative results for various different Reynolds numbers as well as quantitative results to compare the performance of the U-Net with the small model version.

4.1 Qualitative Evaluation

Here, we provide a qualitative analysis of the wakeflow dynamics for different Reynolds numbers and show that our technique is capable of handling the Magnus effect as well as generalizing to new domains not seen during training.

4.1.1 Wakeflow Dynamics

We trained several models to learn the dynamics of fluids with different viscosities and densities. Snapshots of the velocity and pressure fields around an elongated obstacle that were generated by our models are visualized in Figure 2 with Paraview. In the following, we will discuss the produced wake dynamics and pressure fields qualitatively.

The wake dynamics behind an obstacle depend largely on the Reynolds number of a flow field. The Reynolds number is defined as follows:

$$Re = \frac{\rho \|\vec{v}\| D}{\mu} \quad (15)$$

Where ρ and μ are the fluid density and viscosity respectively, $\|\vec{v}\|$ is the flow speed and D the obstacle's diameter. For very small Reynolds numbers (see Figure 2 a)), the flow becomes time-reversible. This means, if we would reverse the simulation, the streamlines would still look the same. This can be recognized by the symmetry of the streamlines before and after the obstacle and the nearly constant pressure gradient. For Reynolds numbers around 10, the fluid starts to form a laminar wake behind the obstacle. This can be seen in Figure 2 b), where 2 vortices are forming behind the obstacle. For Reynolds numbers beyond 100, the wake becomes unstable and vortices generated at the obstacle start to detach and travel downstream. Figure 2 c) ($Re = 800$) clearly shows this turbulent behavior.

4.1.2 Magnus Effect

The Magnus effect appears if a fluid streams around a rotating body. In this case, a high pressure field arises where the surface of the rotating body moves against flow direction and a low pressure field arises where the surface moves along flow direction. In sports such as e.g. soccer or tennis the Magnus effect causes deflections of the path of a spinning ball and it also plays a crucial role for Flettner rotors. In Figure 3, this effect can be clearly recognized.

4.1.3 Generalization

We also tested the model's capability to generalize to new domain geometries that were not contained in the dataset. In particular, we considered the shapes of a car and a fish (see Figure 4). In both cases, our fluid models were able to produce plausible flow and pressure fields (see high pressure fields in front of the obstacles and low pressure as well as turbulent flow behind the obstacles).

To further improve performance on domains not seen during training, it is possible to fine-tune pretrained fluid models.

4.2 Quantitative Evaluation

In the following, we provide quantitative results of our method and investigate the stability of the fluid simulations over time as well as the robustness for different Reynolds numbers.

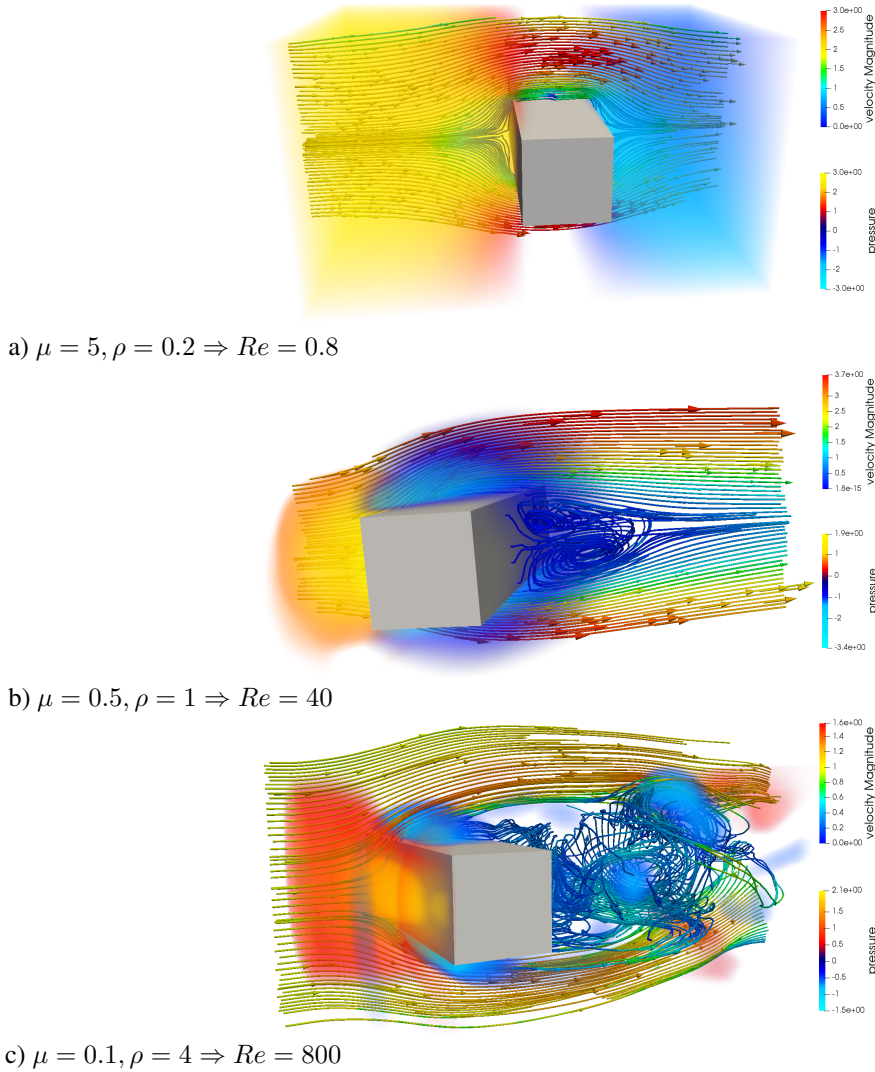
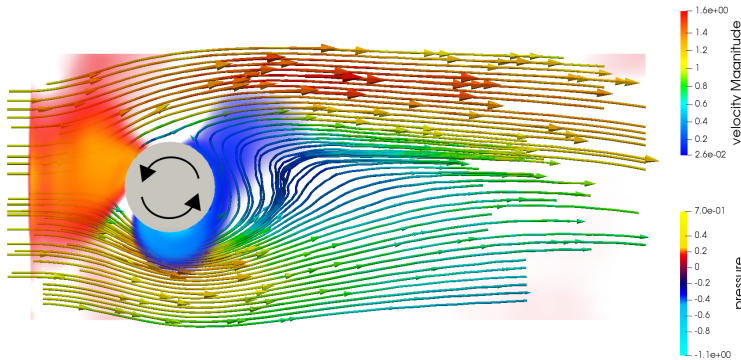
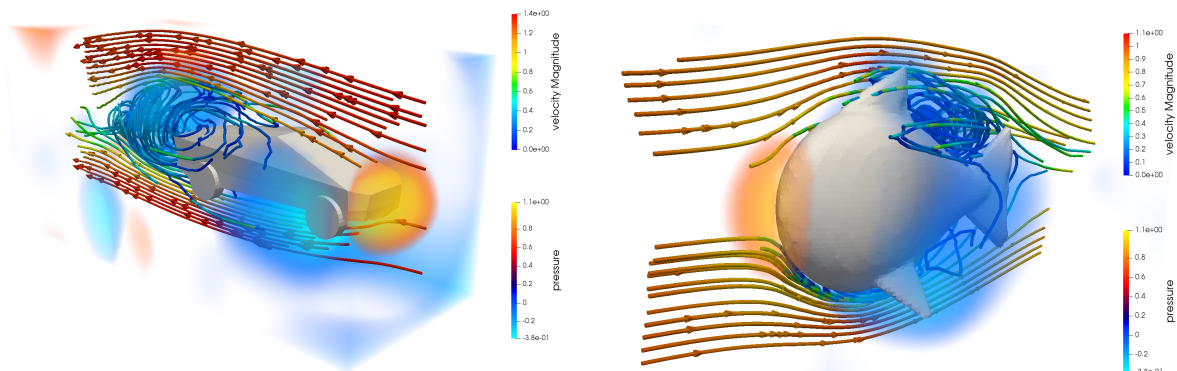


Figure 2: Streamlines and pressure field of flow around square rods at different Reynolds numbers. $\|\vec{v}\| = 1, D = 20$. Generated by the small model and visualized with Paraview.

4.2.1 U-Net vs Small Model

To compare the performance of the U-Net with the small model quantitatively, we measured their speed as well as performance with respect to $E[\|\nabla \cdot \vec{v}\|]$ and L_p on a $128 \times 64 \times 64$ grid (see Table 1). $E[\|\nabla \cdot \vec{v}\|]$ is defined as the mean L_2 norm of the velocity divergence and was averaged from timestep 1500 until timestep 4000. To compute $E[\|\nabla \cdot \vec{v}\|]$, we set the velocity field at the boundaries equal to the boundary conditions. Otherwise, $\nabla \cdot \vec{v}$ would be 0 everywhere. While the U-Net provides highly accurate results for both, $E[\|\nabla \cdot \vec{v}\|]$ and L_p , the small model yields considerably faster solutions and is suitable for real-time simulations. Furthermore, the small model gets along with a drastically reduced number of parameters. Note that a direct comparison to [1] is not possible since their approach only considers Eulerian fluids and therefore does not model viscosity. However, when considering $E[\|\nabla \cdot \vec{v}\|]$ our method indicates significantly lower divergence of the velocity field (by 3 orders of magnitude) - presumably because our method learns a vector field instead of a Helmholtz projection step. Furthermore, our approach is significantly faster than the approach by Um et al. [3]. This may result from the fact that our method does not rely on a differentiable fluid solver. Their method takes 7.6 timesteps per second on a smaller $64 \times 32 \times 32$ fluid-domain. In contrast, our simulation runs at 37 timesteps per second for a domain size of $128 \times 64 \times 64$.

Figure 3: Magnus effect on a counter-clockwise spinning cylinder. ($\mu = 0.5, \rho = 1$)

(a) Exemplary simulation result for car shapes that were not considered in the training set.

(b) Exemplary simulation result for fish shapes that were not considered in the training set.

Figure 4: Generalization examples ($\mu = 0.1, \rho = 4$)

4.2.2 Stability

Figure 5 shows the evolution of $E[||\nabla \cdot \vec{v}||]$ and L_p over time of a simulation performed by the U-Net. Since the simulation starts with $\vec{a}^0 = \vec{0}$ and $p^0 = 0$, it needs several timesteps to warm-up. After about 1500 timesteps, good stability characteristics are shown over thousands of time steps.

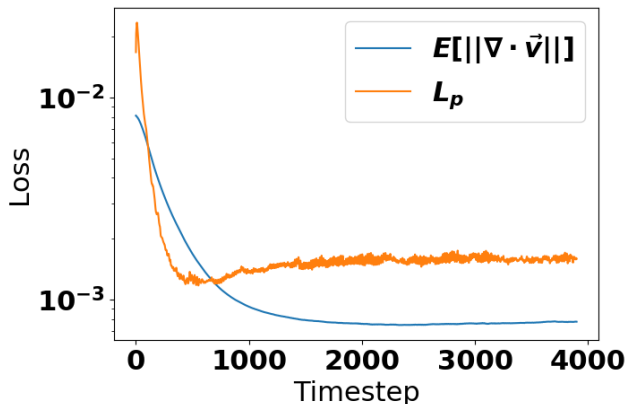
We also investigated the robustness of $E[||\nabla \cdot \vec{v}||]$ for different fluid viscosities and densities (see Table 2). All models were able to find decent solutions. A comparison of L_p is not possible since it directly depends on μ and ρ .

5 Discussion and Outlook

In this work, we propose a novel unsupervised approach of learning incompressible fluid dynamics in 3D. For this purpose, we use the combination of a physics-informed loss function, that penalizes residuals of the Navier Stokes equations on a 3D staggered grid, and an efficient fluid simulation model based on neural network architectures. Our approach allows for fast fluid simulation while taking into account various fluid phenomena such as the Bernoulli effect, Magnus effect and Kármán vortex streets. Furthermore, in contrast to other approaches, our approach does not rely on the availability of vast amounts of data from fluid-solvers such as FEniCS, OpenFOAM or Mantaflow. Our approach

Method	CPU	GPU	$E[\nabla \cdot \vec{v}]$	L_p	n_{params}
U-Net	0.36	14	7.9e-4	1.6e-3	51.6 M
small model	0.89	37	8.75e-4	3.6e-3	1.2 M

Table 1: Quantitative comparison of computational speed in timesteps per second on a CPU and GPU and accuracy with respect to $E[||\nabla \cdot \vec{v}||]$ and L_p . The grid size was $128 \times 64 \times 64$ and $\mu = 0.1, \rho = 4$.

Figure 5: Stability of the U-Net for $\mu = 0.1, \rho = 4$

Method	μ	ρ	$E[\nabla \cdot \vec{v}]$
Small model	5	0.2	1.0e-3
Small model	0.5	1	6.9e-4
Small model	0.1	4	8.75e-4

Table 2: Quantitative results for different fluid viscosities and densities.

generalizes to new domains in 3D and is capable of handling dynamically changing boundary conditions as required for interactive scenarios.

In the future, more sophisticated network architectures could be explored to even further increase the speed and accuracy of the simulation. Furthermore, Neumann boundary conditions could be considered.

References

- [1] Jonathan Tompson, Kristofer Schlachter, Pablo Sprechmann, and Ken Perlin. Accelerating eulerian fluid simulation with convolutional networks. In *Proceedings of the 34th International Conference on Machine Learning-Volume 70*, pages 3424–3433. JMLR. org, 2017.
- [2] Nils Wandel, Michael Weinmann, and Reinhard Klein. Learning incompressible fluid dynamics from scratch - towards fast, differentiable fluid models that generalize. *arXiv preprint arXiv:2006.08762*, 2020.
- [3] Kiwon Um, Raymond Fei, Philipp Holl, Robert Brand, and Nils Thuerey. Solver-in-the-loop: Learning from differentiable physics to interact with iterative pde-solvers, 2020.
- [4] Byungsoo Kim, Vinicius C. Azevedo, Nils Thuerey, Theodore Kim, Markus Gross, and Barbara Solenthaler. Deep fluids: A generative network for parameterized fluid simulations. In *Computer Graphics Forum*, volume 38, pages 59–70. Wiley Online Library, 2019.
- [5] Nicholas Geneva and Nicholas Zabaras. Modeling the dynamics of pde systems with physics-constrained deep auto-regressive networks. *Journal of Computational Physics*, 403:109056, 2020.
- [6] Robert A. Gingold and Joseph J. Monaghan. Smoothed particle hydrodynamics: theory and application to non-spherical stars. *Monthly notices of the royal astronomical society*, 181(3):375–389, 1977.
- [7] L’ubor Ladický, SoHyeon Jeong, Barbara Solenthaler, Marc Pollefeys, and Markus Gross. Data-driven fluid simulations using regression forests. *ACM Trans. Graph.*, 34(6), October 2015.
- [8] Damian Mrowca, Chengxu Zhuang, Elias Wang, Nick Haber, Li Fei-Fei, Joshua B. Tenenbaum, and Daniel L. K. Yamins. Flexible neural representation for physics prediction. In *Proceedings of the 32nd International Conference on Neural Information Processing Systems, NIPS’18*, page 8813–8824, Red Hook, NY, USA, 2018. Curran Associates Inc.
- [9] Yunzhu Li, Jiajun Wu, Russ Tedrake, Joshua B Tenenbaum, and Antonio Torralba. Learning particle dynamics for manipulating rigid bodies, deformable objects, and fluids. In *ICLR*, 2019.

- [10] Benjamin Ummenhofer, Lukas Prantl, Nils Thuerey, and Vladlen Koltun. Lagrangian fluid simulation with continuous convolutions. In *8th International Conference on Learning Representations, ICLR 2020, Addis Ababa, Ethiopia, April 26-30, 2020*. OpenReview.net, 2020.
- [11] Connor Schenck and Dieter Fox. Spnets: Differentiable fluid dynamics for deep neural networks. In *Conference on Robot Learning*, pages 317–335, 2018.
- [12] Justin Sirignano and Konstantinos Spiliopoulos. Dgm: A deep learning algorithm for solving partial differential equations. *Journal of Computational Physics*, 375:1339 – 1364, 2018.
- [13] Philipp Grohs, Fabian Hornung, Arnulf Jentzen, and Philippe Von Wurstemberger. A proof that artificial neural networks overcome the curse of dimensionality in the numerical approximation of black-scholes partial differential equations. *arXiv preprint arXiv:1809.02362*, 2018.
- [14] Yuehaw Khoo, Jianfeng Lu, and Lexing Ying. Solving for high-dimensional committor functions using artificial neural networks. *Research in the Mathematical Sciences*, 6(1):1, 2019.
- [15] Yin hao Zhu and Nicholas Zabaras. Bayesian deep convolutional encoder–decoder networks for surrogate modeling and uncertainty quantification. *Journal of Computational Physics*, 366:415 – 447, 2018.
- [16] Yin hao Zhu, Nicholas Zabaras, Phaedon-Stelios Koutsourelakis, and Paris Perdikaris. Physics-constrained deep learning for high-dimensional surrogate modeling and uncertainty quantification without labeled data. *Journal of Computational Physics*, 394:56 – 81, 2019.
- [17] Rohit K. Tripathy and Ilias Bilonis. Deep uq: Learning deep neural network surrogate models for high dimensional uncertainty quantification. *Journal of Computational Physics*, 375:565 – 588, 2018.
- [18] Cheng Yang, Xubo Yang, and Xiangyun Xiao. Data-driven projection method in fluid simulation. *Computer Animation and Virtual Worlds*, 27(3-4):415–424, 2016.
- [19] Maziar Raissi, Alireza Yazdani, and George Em Karniadakis. Hidden fluid mechanics: A navier-stokes informed deep learning framework for assimilating flow visualization data. *arXiv preprint arXiv:1808.04327*, 2018.
- [20] Nicholas Geneva and Nicholas Zabaras. Quantifying model form uncertainty in reynolds-averaged turbulence models with bayesian deep neural networks. *Journal of Computational Physics*, 383:125 – 147, 2019.
- [21] Julia Ling, Andrew Kurzwaski, and Jeremy Templeton. Reynolds averaged turbulence modelling using deep neural networks with embedded invariance. *Journal of Fluid Mechanics*, 807:155–166, 2016.
- [22] Markus Schöberl, Nicholas Zabaras, and Phaedon-Stelios Koutsourelakis. Predictive collective variable discovery with deep bayesian models. *The Journal of Chemical Physics*, 150(2):024109, 2019.
- [23] Maziar Raissi, P. Perdikaris, and George Em Karniadakis. Physics-informed neural networks: A deep learning framework for solving forward and inverse problems involving nonlinear partial differential equations. *Journal of Computational Physics*, 378:686 – 707, 2019.
- [24] Francis H. Harlow and J. Eddie Welch. Numerical calculation of time-dependent viscous incompressible flow of fluid with free surface. *The physics of fluids*, 8(12):2182–2189, 1965.
- [25] Jos Stam. Stable fluids. In *Proceedings of the 26th annual conference on Computer graphics and interactive techniques*, pages 121–128, 1999.
- [26] Junhyuk Kim and Changhoon Lee. Deep unsupervised learning of turbulence for inflow generation at various reynolds numbers. *Journal of Computational Physics*, 406:109216, 2020.
- [27] You Xie, Erik Franz, Mengyu Chu, and Nils Thuerey. Tempogan: A temporally coherent, volumetric gan for super-resolution fluid flow. *ACM Trans. Graph.*, 37(4), July 2018.
- [28] Nils Thuerey, Konstantin Weißenow, Lukas Prantl, and Xiangyu Hu. Deep learning methods for reynolds-averaged navier–stokes simulations of airfoil flows. *AIAA Journal*, pages 1–12, 2019.
- [29] H. O’Reilly and Jeffrey M. Beck. A family of large-stencil discrete laplacian approximations in three dimensions. *International Journal For Numerical Methods in Engineering*, 2006.
- [30] Özgün Çiçek, Ahmed Abdulkadir, Soeren S. Lienkamp, Thomas Brox, and Olaf Ronneberger. 3d u-net: Learning dense volumetric segmentation from sparse annotation. *CoRR*, abs/1606.06650, 2016.
- [31] Diederik P. Kingma and Jimmy Ba. Adam: A method for stochastic optimization. In *3rd International Conference on Learning Representations, ICLR 2015, San Diego, CA, USA, May 7-9, 2015, Conference Track Proceedings*, 2015.